Dielectric function model for *p*-type semiconductor inter-valence band transitions

Yan-Feng Lao and A. G. Unil Perera[a]
Department of Physics and Astronomy, Georgia State University, Atlanta, Georgia 30303, USA

The contributions of inter-valence band (IVB) transitions to the dielectric function (DF) by free holes among the split-off (so), light-hole (lh) and heavy-hole (hh) bands were investigated. A model was developed to determine the DF of two *p*-type semiconductors, GaAs and $Ge_{1-y}Sn_y$ with the Zinc-blend and Diamond crystal structures, respectively. The IVB transitions dominate the spectral range between 0.1–1eV with respect to the spin-orbit splittings between so-hh and lh-hh bands. In conjunction with inter-band transitions, free-carrier and lattice absorption, a complete DF model allows the determination of optical constants with improved accuracy in the spectral range covering both ultraviolet and infrared regions. The model should be applicable to most of the group III-V and IV materials since their valence band structures resemble the ones under investigation. © *2011 American Institute of Physics*. [doi:10.1063/1.3590138]

I. INTRODUCTION

The optical response of semiconductors can be described by the dielectric function (DF) which is determined in terms of various optical processes, such as band-to-band (BB) transitions, photon-phonon interactions (lattice absorption), intra-band and inter-valence band (IVB) transitions in the presence of free holes. For BB transitions, critical points (CPs) are known to play an important role in the DF[1] as the associated joint density of states (JDOS) exhibits strong variations with photon energies in the vicinity of CPs. The analytical form of the DF can be deduced in terms of singularity types according to the behavior of JDOS expanded into polynomial k terms around CPs. The resulting DF is known as the Adachi's model dielectric function (MDF).[1] In addition, Elliott[2] presented a theory considering the electron-hole Coulomb interactions under the approximation of isotropic parabolic bands. The DF model[3] is thus, derived with the absorption of Wannier excitons which includes discrete excitonic lines below the bandgap and a continuum of absorption above the bandgap. Both models have successfully presented the DF in a variety of materials.[1,4] However, only inter-band transitions [referred as Band to Band (BB) transitions below], i.e., from the valence bands (VBs) to the conduction band (CB), are considered to account the DF measured on intrinsic materials. In the presence of free holes, two effects, i.e., intra-band indirect [referred as free carrier (FC) below] and IVB direct transitions, contribute to the DF. The DF modeling of FC absorption based on the classic Drude theory[5] has been employed for doped materials in previous works[6–9] showing good agreement with experiments, whereas, IVB modeling receives less attention.

In a semiconductor where free holes are present, IVB transitions can occur among the split-off (so), light-hole (lh) and heavy-hole (hh) bands each with two-fold spin degeneracy.

Each pair of transitions produces a characteristic absorption peak, leading to three separate peaks as observed in lightly doped samples.[10] Recently, highly *p*-doped semiconductors have attracted attention for optical studies on the absorption properties[11,12] and the infrared DF[13] as well as applications to hetero-junction internal photoemission detectors.[14–16] As both IVB and FC absorption depend on the concentration of free holes, total absorption coefficient (α) of heavily doped materials can be higher than that based on BB transitions in the same spectral region, e.g., the HgCdTe ternary alloy.[17] As far as the absorption properties is concerned, highly *p*-doped semiconductors would be attractive for several applications. For instance, recent works[15,16] as demonstrated in internal photoemission type detectors[14] have shown infrared detection capability from the short-wave[15] (1–3 μm) to the long-wave[16] infrared (8–14 μm) range at high operating temperatures (up to 330K). Therefore, a model dealing with the IVB transitions will be of interest for practical applications as well as for fundamental research, since the doping scheme is essential for semiconductor structures. Furthermore, accurate simulation and design of structures need proper handling of doping effects including the IVB transitions for calculating optical constants.

A straightforward approach regarding IVB absorption is to start from band-structure calculations.[18,19] Under the framework of $k \cdot p$ perturbation theory, Kane[18] presented a three-band model and calculated absorption spectra for *p*-type Ge and Si. A more accurate handling of the VB structure was performed by Arthur *et al.*[19] with an 18×18 $k \cdot p$ treatment. Since transitions between energy states near the Γ point are primarily responsible for optical absorption, a proper approximation to the VB around Γ point, as opposed to complete presentation in the entire BZ, should be sufficient, which brings about the parabolic-band approximation. This feasibility was illuminated in Kahn's work.[20] However, Kahn's formula was deduced with the Boltzmann statistics and no line-shape broadening was considered, which is the

[a]Electronic mail: uperera@gsu.edu.

109, 103528-1
© 2011 American Institute of Physics

case for lower doped samples. The presence of dopants enhances carrier scattering probability, resulting in a relaxation of the selection rule and hence the line-shape broadening.[21] For the DF model being able to be applicable to high doping levels, these factors need to be addressed.

In this work, a DF model for IVB transitions was deduced with analytical expressions under the parabolic-band approximation. In addition to Kahn's works,[20] Huberman *et al.*[11] calculated the lh-hh absorption to interpret their measurements on highly *p*-doped GaAs. Songprakob *et al.*[12] calculated the optical matrix element based on analytical expressions deduced by Kane[18] and incorporated the Lorentzian oscillator-type broadening. D'Costa *et al.*[13] used two or three Gaussian oscillators to fit to their measured spectra depending on the number of observed peaks. All these studies concentrate on the highly doped cases ($> 10^{19} \mathrm{cm}^{-3}$). This work starts from the exact expression[22] of the DF imaginary component (ε_2) by applying parabolic-band approximation. The deduced DF is able to fit to different materials with varied doping concentrations from low values (e.g., $10^{16} \mathrm{cm}^{-3}$) up to $10^{20} \mathrm{cm}^{-3}$. In contrast to reported absorption spectra,[11,12] the current model gives the complex DF of *p*-type GaAs which will be useful for device design. A strength constant empirically involves the momentum matrix element and results from the fitting to experiments. The line-shape broadening is introduced using the method similar to that of BB transitions.[3] The discussing IVB model completes the complex DF with other contributions from BB transitions, FC and lattice absorption, resulting in the fitting for a wide range of photon energies, namely, 0.01–6eV in this work. The DF of two representative *p*-type semiconductors, GaAs and $\mathrm{Ge}_{1-y}\mathrm{Sn}_y$ with the Zinc-blend and Diamond types of crystal structures, respectively, was determined. The $\mathrm{Ge}_{1-y}\mathrm{Sn}_y$ grown on Si substrate was recently reported by D'Costa *et al.*,[13] showing promising applications in optical communications combined with the capability of electronic circuits on the Si platform. The DF model can be used to determine related optical constants, e.g., the index of refraction, for various doping concentrations and is thus, desirable for such applications. The model will be expected to be applicable to most of the group III-V and IV semiconductors, such as InP which has a similar band structure to the GaAs but having a smaller spin-orbit splitting energy, i.e., $\Delta_0(\mathrm{InP}) = 0.108$ eV.[23]

II. THEORETICAL MODELS

As the real (ε_1) and imaginary (ε_2) components of the DF are connected by the Kramers-Kronig (KK) relations, the calculation of ε_2 needs to consider optical processes in the entire spectral range to accurately determine the ε_1. The DF model including BB transitions above the bandgap and IVB transitions, FC and lattice absorption below the bandgap will be addressed in this Section.

A. Analytical DF model for IVB transitions

The contribution of optical transitions to the imaginary component of the DF can be expressed by[22]

$$\varepsilon_2(E) = \frac{\hbar^2 e^2}{8\pi^2\varepsilon_0 m_0^2 E^2} \sum_{i,j} \int_{BZ} d\boldsymbol{k} \overline{|\hat{e}\cdot\boldsymbol{p}_{ij}|^2}$$
$$\delta[E_j(\boldsymbol{k}) - E_i(\boldsymbol{k}) - E](f_i - f_j) \quad (1)$$

where E is the photon energy, $\hbar$ is the Planck constant, e and m_0 are the charge and mass of a free electron, ε_0 is the vacuum permittivity, $\boldsymbol{k}$ is the wave vector at which hole transitions are occurring, $\hat{e}$ is a unit vector in the direction of the optical electric field, p_{ij} is the momentum matrix element, the δ function denotes energy conservation involved, $E_{i(j)}(k)$ is the energy of states for band $i(j)$, and $f_{i(j)}$ is the hole Fermi-Dirac (FD) distribution function representing occupation probability. A factor of two due to two-fold spin degeneracy is not explicitly included. Therefore, i and j represent the indices of energy states with different spin states distinguished for one band.

The momentum matrix element depends on the polarization of the optical electromagnetic field. In a bulk material, photons interact with electrons with k pointing all kinds of directions. The resulting matrix element should be averaged with respect to the solid angle $d\Omega$ given by

$$\overline{|\hat{e}\cdot\boldsymbol{p}_{ij}|^2} = \frac{1}{4\pi}\int|\hat{e}\cdot\boldsymbol{p}_{ij}|^2 d\Omega \equiv P_x^2 F_{ij}(k) \quad (2)$$

P_x is defined as the matrix element of the momentum operator between the *s*-like ($|s\rangle$) and *p*-like wave functions ($|x\rangle$, $|y\rangle$ and $|z\rangle$), and associated with energy parameter E_P. $F_{if}(k)$ is a dimensionless quantity. The δ function in Eq. (1) can be integrated out, resulting in a two-dimensional (2D) integration over a constant-energy surface. For each IVB transitions, only F_{ij} is related to the energy states as associated bands are in two-fold spin degeneracy. As such, total IVB contributions can be expressed as

$$\varepsilon_2(E) = \varepsilon_2^{12}(E) + \varepsilon_2^{13}(E) + \varepsilon_2^{23}(E) \quad (3)$$

where the terms in order correspond to the lh-hh, so-hh and so-lh transitions, respectively, with the form

$$\varepsilon_2^{ab}(E) = \frac{C_0}{E^2} \oiint \frac{dS_k}{|\nabla_k E(\boldsymbol{k})|} F_{ab}(\boldsymbol{k})(f_a - f_b) \quad (4)$$

in which $C_0 = \hbar^2 e^2 E_P / (16\pi^2 \varepsilon_0 m_0)$ and indices $a(b) = 1$, 2 and 3 denote the hh, lh and so bands, respectively. The choice for the combinations of a and b has been shown in Eq. (3). dS_k is the elemental area on the constant-energy surface, and $\nabla_k E(\boldsymbol{k})$ is the gradient of transition energy. The Fermi-Dirac distribution function for holes $f_{a(b)}$ is only determined by the energy with the expression $f_{a(b)} = \left[1 + \exp\left(\frac{E_f - E_{a(b)}}{k_B T}\right)\right]^{-1}$, where E_f is the energy of the hole quasi-Fermi level. Notice that $\boldsymbol{k}$ is determined in terms of $E_a(\boldsymbol{k}) - E_b(\boldsymbol{k}) = E$. For one $\boldsymbol{k}$ value, there are two degenerated energy states in each bands. $F_{ab}(\boldsymbol{k})$ is thus, defined as the summation $\sum_{i,j} F_{ij}(\boldsymbol{k})$ with i and j the energy-state indices. As for one transition from band a to band b, contributions from four transitions are summed to calculate the F_{ab}.

To deduce analytical form of Eq. (4), approximation to $F_{ab}(\boldsymbol{k})$ is required. To view the variation of F_{ab} with the

wave vector k, the $\boldsymbol{k} \cdot \boldsymbol{p}$ method based on an 8×8 Hamiltonian reported by Bahder[24] was used to compute F_{ab} as shown in Fig. 1. Around the Γ point ($\boldsymbol{k} = 0$), $F_{ab}(\boldsymbol{k})$ is approximately proportional to k^2, which is the similar result of isotropic parabolic-band approximation used by Kahn.[20] Assuming $F_{ab}(k) = B_{ab}k^2$ and the parabolic-band structure $E_a(\boldsymbol{k}) = -E_{a0} - \hbar^2 k^2 / 2m_a^*$, where B_{ab} is a constant parameter, E_{a0} is the band-edge energy and m_a^* is the effective mass, Eq. (4) becomes

$$\varepsilon_2^{ab}(E) = A_{ab} \frac{|E - (E_{b0} - E_{a0})|^{\frac{3}{2}}}{E^2} \frac{p}{(k_B T)^{\frac{3}{2}}}$$
$$\left[\exp\left(\frac{E_a}{k_B T} \right) - \exp\left(\frac{E_b}{k_B T} \right) \right] \cdot C_{FD}^{ab}. \quad (5)$$

Here, p is the hole concentration. A_{ab} and C_{FD}^{ab} have the following expressions,

$$A_{ab} = \frac{16 C_0 B_{ab}}{\hbar^2 (m_1^{*3/2} + m_2^{*3/2})} \left(\frac{\pi m_a^* m_b^*}{|m_a^* - m_b^*|} \right)^{\frac{5}{2}} \quad (6)$$

$$C_{FD}^{ab} = \frac{\exp\{-[E_f + k_B T \ln(\frac{P}{N_v})]/k_B T\}}{\{1 + \exp[(E_a - E_f)/k_B T]\}\{1 + \exp[(E_b - E_f)/k_B T]\}} \quad (7)$$

with N_v the sum of hh and lh effective density of states calculated by $N_v = 2(k_B T / 2\pi \hbar^2)^{3/2} (m_1^{*3/2} + m_2^{*3/2})$. For low doping concentrations, E_f lies above the VB top, yielding $C_{FD}^{ab} \approx 1$, which is the case of applying the Boltzmann statistics.[20] Notice that constant m^* used in parabolic-band approximation gives fixed values of A_{ab}. Whereas, the nonparabolicity as in the actual VBs off the Γ point causes varied m^* and hence A_{ab}. At wave vectors where hole transitions will see the parallel bands, A_{ab} can be significantly increased.

As shown in Fig. 1(d), F_{12} has a maximum value. At high photon energies (large k), F_{12} is reduced as k increases.
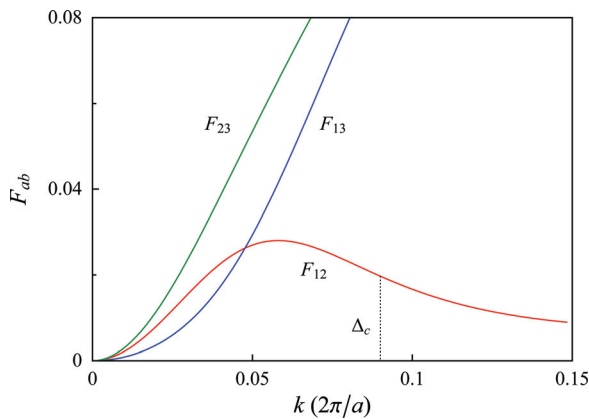
In parabolic band approximation, such behavior is considered by setting a cutoff energy Δ_c for the lh-hh transition above which the F_{12} is set to zero. In terms of fitting results (see Fig. 3), the Δ_c corresponds to k values greater than the maxima in Fig. 1(d). To be able to compare with the experiment, the unbroadening DF [Eq. (5)] is convoluted with a line-shape function[3] as below,

$$\varepsilon_2^{ab(\Gamma)}(E) = \int_0^{+\infty} dE' \, \varepsilon_2^{ab}(E') [L_{ab}(E', E) - L_{ab}(-E', E)] \quad (8)$$

in which L_{ab} is a broadening function with the Lorentzian line shape,

$$L_{ab}(E', E) = \frac{1}{\pi} \frac{\Gamma_{ab}}{(E - E')^2 + \Gamma_{ab}^2} \quad (9)$$

where Γ_{ab} is a broadening constant.

In addition to the Lorentzian function, Gaussian[13,25] and Sech[26] functions have been also used as the broadening line shapes according to the underneath mechanisms. It was believed that crystal strain and impurities cause the Gaussian broadening,[13,25] while the radiative lifetime broadening and thermal effects have the Lorentzian nature. However, a critical difference from one to one is not evident. For instance, the Lorentzian broadening was successfully applied for IVB transitions.[11,12] The actual situation could be a mixing effect in one experiment, e.g., impurities, thermal effects etc., which obscures the difference. In our case, a Lorentzian line-shape function [Eq. (9)] was applied to p-type GaAs by following previous works on highly doped GaAs.[11,12] For $Ge_{1-y}Sn_y$ on Si substrates, the presence of a tensile strain of 0.15% in the film results in best fit with a Gaussian line,[13] which indicates the following broadening function,
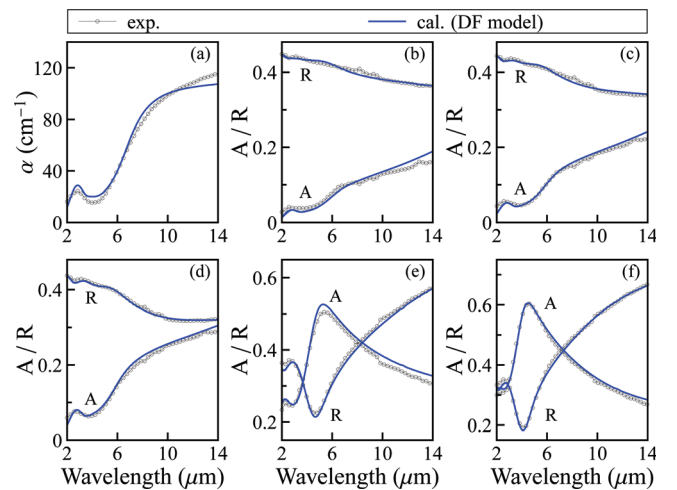

FIG. 1. (Color online) The variation of calculated F_{ab} by the 8×8 $\boldsymbol{k} \cdot \boldsymbol{p}$ method with the magnitude of wave vectors. F_{ab} is a dimensionless quantity proportional to the squared momentum matrix element. A cutoff energy parameter Δ_c is defined for the lh-hh transition to apply the parabolic-band approximation. The subscripts 12, 13 and 23 represent the lh-hh, so-hh and so-lh transitions, respectively.

FIG. 2. (Color online) The comparison of experimental and calculated spectra for p-GaAs. In (a), theoretical values of absorption coefficient (α) are compared with the measurement taken from Ref. 32. All other curves are in terms of the absorption (A) and reflection (R). The doping concentrations of samples in (a)–(f) are 2.7×10^{17}, 3.0×10^{18}, 4.7×10^{18}, 7.1×10^{18}, 6.6×10^{19}, $1.1 \times 10^{20} cm^{-3}$, respectively, where the data of samples (e) and (f) are taken from Ref. 12.
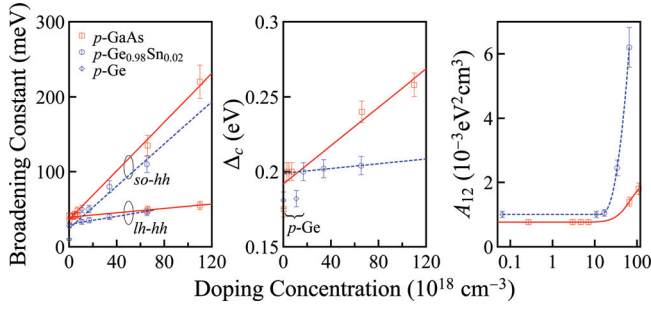
FIG. 3. (Color online) The Fitting parameters for calculating IVB contributions to the DF. Δ_c and A_{12} are the cutoff and strength parameters, respectively, for the lh-hh transition. The fitting process is described in the text. An additional sample of p-type Ge$_{0.98}$ Sn$_{0.02}$ doped at 1.68×10^{19}cm^{-3} which is not shown in Fig. 5, is adopted from Ref. 13.

$$L_{ab}(E', E) = \frac{1}{\sigma_{ab}\sqrt{2\pi}} \exp\left[\frac{(E-E')^2}{2\sigma_{ab}^2}\right] \quad (10)$$

where σ_{ab} is a Gaussian broadening parameter.

B. The contributions of BB transitions to the DF

The BB transitions take place at photon energies greater than the bandgap and influence the DF in the region below the bandgap via the KK relations. The absorption lines around the CPs are usually affected by the electron-hole Coulomb attraction which results in discrete excitonic lines below the CP edge. For high temperatures (e.g., room temperatures) or in intentionally doped semiconductors, the excitonic effects can be strongly damped leaving the Coulomb enhancement effects on the BB transitions, which is known as the band-to-band Coulomb enhancement (BBCE) effects.[4] Elliott[2] and several others[3,4] considered such effects and are thus, adopted here. In the following, the DF is calculated by summing contributions from three sets of CPs. Detailed discussions can be found in Refs. 2–4.

For the E_0 transition, ε_2 is given by[3]

$$\varepsilon_2(E) = \frac{2\pi A\sqrt{R_0}}{E^2}\left\{\sum_{n=1}^{+\infty}\frac{2R_0}{n^3}\delta(E-E_{n,0}^{ex}) + \frac{\theta(E-E_0)}{1-\exp[-2\pi\sqrt{R_0/(E-E_0)}]}\right\} \quad (11)$$

with excitonic energy $E_{n,0}^{ex} = E_0 - R_0/n^2$,[3,4] $n = 1, 2,....$ R_0 is the effective Rydberg energy, θ is the Heaviside function. The broadening will follow the Lorentzian formula Eqs. (8) and (9). For excitonic continuum and discrete lines, broadening constants are named as Γ_0 and $\Gamma_{n,0}^{ex}$, respectively, with the relationship $\Gamma_{n,0}^{ex} = \Gamma_0 - (\Gamma_0 - \Gamma_{1,0}^{ex})/n^2$ (Ref. 4). The DF for the $E_0 + \Delta_{so}$ transition has a similar form with the replacement $A \rightarrow B$, $E_0 \rightarrow E_0 + \Delta_{so}$, $R_0 \rightarrow R_{so}$, $\Gamma_0 \rightarrow \Gamma_{so}$, and $\Gamma_{n,0}^{ex} \rightarrow \Gamma_{n,so}^{ex}$.

For the E_1 transition, ε_2 is given by[3]

$$\varepsilon_2(E) = \frac{2C_1}{E^2}\left\{\sum_{p=0}^{+\infty}\frac{2R_1}{(p+1/2)^3}\delta(E-E_{p,1}^{ex}) + \frac{\theta(E-E_1)}{1+\exp[-2\pi\sqrt{R_1/(E-E_1)}]}\right\} \quad (12)$$

with $E_{p,1}^{ex} = E_1 - R_1/(p + \frac{1}{2})^2$,[3,4] $p = 0, 1, ...$ R_1 is the 2D Rydberg energy. For the E_1 transitions, same broadening for excitonic continuum and discrete lines was used as Γ_1 (Ref. 4). Also, the DF for the $E_1 + \Delta_1$ transition has a similar form to Eq. (12) with the replacement $C_1 \rightarrow C_2$, $E_1 \rightarrow E_1 + \Delta_1$, $R_1 \rightarrow R_{\Delta_1}$, and $\Gamma_1 \rightarrow \Gamma_{\Delta_1}$. The same Rydberg energy will be used for E_1 and $E_1 + \Delta_1$ transitions, i.e., $R_1 = R_{\Delta_1}$ (Ref. 4). Notice that the term $1/E^2$ in Eqs. (11) and (12) will be integrated during applying the broadening formula (Eq. 8). The DF calculated here follows the works of Tanguy,[3] i.e., Eqs. (1) and (3) of Ref. 3.

The contributions of other higher-lying transitions to the DF are usually modeled as damped harmonic oscillator terms:[4]

$$\varepsilon(E) = \varepsilon_1(E) + i\varepsilon_2(E) = \frac{F(j)}{(1-\chi_j^2) - i\chi_j\gamma(j)} \quad (13)$$

where $\chi_j = E/E_j$, E_j is the transition energy, $F(j)$ and $\gamma(j)$ are the dimensionless strength and damping constant, respectively.

C. FC and lattice absorption

The interaction of photons with phonons and free carriers falls into the far infrared region. The coupling of electromagnetic waves to the transverse optical (TO) phonon modes in a polar crystal can be modeled as harmonic oscillators,[5] while treatment of FC absorption with the Drude theory[5] has resulted in good agreement with experiments.[9] The resultant DF have the following form as reported previously:[7–9]

$$\varepsilon(\omega) = \varepsilon_\infty\left[1 - \frac{\omega_p^2}{\omega(\omega + i\gamma)}\right] + \frac{S \cdot \omega_{TO}^2}{\omega_{TO}^2 - \omega^2 - i\omega\Gamma} \quad (14)$$

where ω is the light frequency in wave numbers, ε_∞ is the high-frequency dielectric constant, ω_p and γ are the plasmon frequency and damping constant, ω_{TO} and Γ are the TO phonon frequency and damping constant. S denotes the oscillator strength expressed by $S = \varepsilon_\infty(\omega_{LO}^2 - \omega_{TO}^2)/\omega_{TO}^2 = \varepsilon_s - \varepsilon_\infty$ to which the Lyddane-Sachs-Teller (LST) relationship[5] $\varepsilon_s = \varepsilon_\infty\omega_{LO}^2/\omega_{TO}^2$ has been applied. ε_s is the static dielectric constant and ω_{LO} is the longitudinal optical (LO) phonon frequency. For nonpolar semiconductors, such as the group IV semiconductors, the LO and TO modes have the same value giving a trivial contribution. For alloyed materials, e.g., Al$_x$Ga$_{1-x}$As, simple sums of multiple phonon terms with different frequency and strength for individual Al-As and Ga-As bonds can be applied.[9]

Notice that the frequency in Eq. (14) is defined as the inverse of wavelength (in cm^{-1}). The plasma frequency and damping constant are thus expressed by

$$\omega_p = \sqrt{\frac{pe^2}{\varepsilon_0\varepsilon_\infty m^*}}\bigg/ 2\pi c \quad (15)$$

and

$$\mu_{IR} = \frac{e\langle\tau\rangle}{m^*} \quad (16)$$

with m^* the effective mass, and $\langle\tau\rangle$ the average scattering time which is related to the damping constant by $\gamma = 1/2\pi c\langle\tau\rangle$. A factor $(2\pi c)$ is used to convert the unit of s^{-1} to cm^{-1}. The effective mass is taken as an average of hh and lh masses,[12] $(m_{lh}^{3/2} + m_{hh}^{3/2})/(m_{lh}^{1/2} + m_{hh}^{1/2})$. In Eq. (16), μ_{IR} represents an optical estimate of the hole mobility which differs the measured mobility in Hall measurements by a factor r_{Hall}, as discussed by Songprakob et al.[12] The values of r_{Hall} used in calculations will be described in Sec. III A.

D. The total DF of p-type semiconductors

As required by KK relations being satisfied between the ε_1 and ε_2, ε_2 was calculated by summing all contributions from IVB transitions [Eq. (4) or (5)], BB transitions [Eqs. (11), (12) and (13)], FC and lattice absorption (Eq. 14) and then introducing the broadening (Eq. 8). The ε_1 was then computed via the KK relationships, i.e.,

$$\varepsilon_1(E) = \varepsilon_{1\infty} + \frac{2}{\pi}\mathcal{P}\int_0^{+\infty} \frac{E'\varepsilon_2(E')}{E'^2 - E^2} dE' \qquad (17)$$

where $\mathcal{P}$ denotes the principal value of the integral. A constant $\varepsilon_{1\infty}$ (Ref. 4), which could be other than unity, was used to account for the vacuum plus contributions from other higher-lying transitions not considered in the DF.

Each optical processes under consideration have the individual dominating rang within which major contributions to the DF are involved. To calculate the IVB DF, the DF in undoped materials with BB and phonon contribution alone is firstly determined.

III. RESULTS AND DISCUSSIONS

Adjustable constants in the DF model (e.g., A_{ab}, Γ_{ab} for IVB transitions, A, B, C_1, C_2 and Γ_0, Γ_{so}, Γ_1, Γ_{Δ_1} for BB transitions) were determined by comparing resultant model spectra with the experimental curves. Direct fit can be applied to the measured DF data. Whereas, infrared measurements with respect to absorption (A), reflection (R) and transmission (T) ($A = 1 - R - T$) are used instead in the situation where DF data are unavailable.

The calculations of A-R-T spectra generally concerns specific configuration of a structure consisted of multiple layers. For the case of thin films on a thick substrate (in the order of magnitude of 10^2 μm), calculations based on an intensity-transfer-matrix method (ITMM) can be carried out. A detailed description can be found in Ref. 12. In this method, the stratified films are dealt with a regular transfer-matrix method (TMM)[27] while multiple reflected beams from the substrate surfaces are added incoherently to neglect the phase information.

The analytical DF model was first applied to p-type GaAs. The undoped GaAs has been studied to a large extent with the well-measured DF data. After the determination of fitting parameters for BB transitions, fit to infrared spectra of p-type GaAs was made using the ITMM. The final DF was calculated in the spectral range between 0.01–6eV for doping concentrations up to 10^{20}cm^{-3}. Thereafter, the model was

applied to a group IV material, $Ge_{1-y}Sn_y$. All experimental data are implied to be taken at room temperature.

A. Application of the DF model to p-type GaAs

The main contributions to the DF in undoped GaAs come from BB transitions and the lattice absorption. Based on the DF model in Sec. II B and the phonon calculation in Sec. II C, a fit to the DF data taken from Zollner's work[28] is shown in the insets of Fig. 4. Table I lists the resulting parameters. A linear increased broadening constant[29] with the doping for the E_0 transition has been used, which was obtained by fitting the experimental data of refract index of p-type GaAs measured by Sell et al.[30]

The phonon parameters listed in Table II are taken from standard database[31] and remain fixed for all doped samples.[9] Calculations involving both BB and phonon contributions allow an accurate determination on the refractive index up to the far infrared region as shown in Fig. 8(a). The efforts in modeling the DF of undoped GaAs provide a baseline above which additional features in the presence of free holes account for IVB contributions.

As no experimental DF data are available for p-type GaAs, A-R-T measurements are adopted. Three 1 μm-thick p-type $Al_{0.01}Ga_{0.99}As$ epilayers[9] grown on 520-μm-thick, double-side polished, semi-insulating GaAs (100) substrates were employed. The films were doped with Be at 3.0×10^{18}, 4.7×10^{18} and 7.1×10^{18}cm^{-3}, respectively. Figure 2 plots the infrared spectra measured using a Perkin-Elmer system 2000 Fourier Transform InfraRed (FTIR) spectrometer. Also shown are the data from the works of Braunstein[32] and Songprakob et al.[12] with which a doping range of up to 10^{20}cm^{-3} can be covered. The Al fraction of 0.01 will cause an increase of 15 meV in the fundamental band gap.[23] According changes in VB-related parameters are small, e.g., the reduction of Δ_0 less than one meV,[23] and can be neglected.
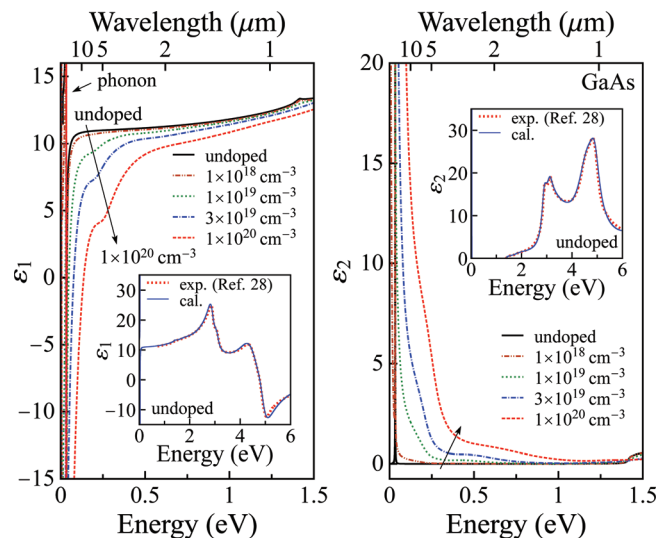

FIG. 4. (Color online) The calculated DF (ε_1 and ε_2) for p-type GaAs at various doping concentrations. The phonon absorption induces a strong feature at the low-energy region. The FC contribution shows a $1/E^2$ behavior. The IVB transitions are responsible for the region between 0.1–1eV. The insets show the calculated DF of undoped GaAs in comparison with experimental data taken from Ref. 28.

TABLE I. Material parameters for computing the contributions of BB transitions to the DF. p denotes the doping concentration (in cm^{-3}). Only the doping-dependent damping of the E_0 transition was considered for GaAs. For Ge and $Ge_{0.98}Sn_{0.02}$, constant damping parameters were used.

	GaAs	Ge	$Ge_{0.98}Sn_{0.02}$
A ($eV^{1.5}$)	2.3 ± 0.1	1.0 ± 0.1	1.0 ± 0.1
E_0 (eV)	1.423^a	0.805 ± 0.005	0.725^b
R_0, R_{so} (meV)	3.4^c	1.6^d	1.6^e
Γ_0 (meV)	$10.4 + 3.2p/10^{18}$	8 ± 2	25 ± 5
B ($eV^{1.5}$)	2.6 ± 0.1	2.5 ± 0.1	2.2 ± 0.1
$E_0 + \Delta_0$ (eV)	1.764^f	1.105 ± 0.005	1.03^g
Γ_{so} (meV)	60 ± 5	50 ± 5	90 ± 5
C_1 (eV^2)	64.0 ± 0.5	65.5 ± 0.5	57.0 ± 0.5
E_1 (eV)	$2.96^{h,i}$	2.12^h	2.07^j
R_1, R_{Δ_1} (meV)	16 ± 5	5 ± 3	5 ± 3
Γ_1 (meV)	120 ± 10	100 ± 10	130 ± 10
C_2 (eV^2)	37.0 ± 0.5	29.0 ± 0.5	33.0 ± 0.5
$E_1 + \Delta_1$ (eV)	3.19^h	2.34^h	2.28^j
Γ_{Δ_1} (meV)	120 ± 10	100 ± 10	130 ± 10
$F(E_0')$	0.60 ± 0.02	0.05 ± 0.02	0.1 ± 0.05
E_0' (eV)	4.44^h	3.14^h	3.10^j
$\gamma(E_0')$	140 ± 10	150 ± 20	160 ± 20
$F(E_0' + \Delta_0')$	1.4 ± 0.02	0.60 ± 0.05	0.70 ± 0.05
$E_0' + \Delta_0'$ (eV)	4.63^h	3.34^h	3.30 ± 0.02
$\gamma(E_0' + \Delta_0')$	140 ± 10	150 ± 20	160 ± 20
$F_2(E_2)$	1.4 ± 0.02	3.0 ± 0.1	3.1 ± 0.1
E_2 (eV)	4.90 ± 0.01	4.28 ± 0.01	4.25 ± 0.01
$\gamma(E_2)$	100 ± 10	140 ± 10	140 ± 10
$F(E')$	0.50 ± 0.02	1.6 ± 0.1	1.8 ± 0.1
E' (eV)	6.6 ± 0.1	3.75 ± 0.05	3.72 ± 0.05
$\gamma(E')$	150 ± 10	200 ± 20	200 ± 20
$\varepsilon_{1\infty}$	0.74	1.25	1.35

[a]Reference 34.
[b]Reference 35.
[c]Calculated by the Eq. (9) of Ref. 25.
[d]Reference 41.
[e]Same as Ge.
[f]In terms of Δ_0 (GaAs) = 0.341 eV (Ref. 23).
[g]With Δ_0 ($Ge_{0.98}Sn_{0.02}$) = 0.30 eV (Ref. 35).
[h]Reference 42.
[i]See data in Table III of Ref. 34.
[j]Reference 35.

Also previous work in the far infrared region[9] has shown negligible AlAs-like phonon effects, which allows the samples to be modeled as p-type GaAs.

The FC contribution was calculated with the parameters of plasma frequency and damping constant [Eq. (14)].

TABLE II. Material parameters for computing the contributions of FC and phonon absorption to the DF (Eq. 14).

Parameter	GaAs	$Ge_{0.98}Sn_{0.02}$
ε_s	13.18^a	16.2^b
ε_∞	10.89^a	16.2^c
ω_{TO} (cm^{-1})	268.0^a	—
Γ_{TO} (cm^{-1})	2.5^d	—

[a]Reference 31.
[b]Reference 22.
[c]In terms of the LST relation (see Sec. II C).
[d]Reference 12.

Related calculations are the determination of averaged effective mass (Table III) considering both the hh and lh bands and the scattering time derived from the mobility[33] [Eq. (16)]. Songprakob et al.[12] discussed a Hall factor r_{Hall} elucidating the dichotomy between the optical and electrical parameters, i.e., $\mu_{IR} = \mu_{Hall}/r_{Hall}$ and $p_{IR} = r_{Hall}p_{Hall}$ (Ref. 12). They obtained a value close to unity (1.2 for μ and 0.9 for p).[12] In this work, r_{Hall} is set to one except calculations (only for the mobility) on the spectra from Songprakob's work[12] where r_{Hall} varying between 1.2–1.4 was used.

IVB parameters are determined by fitting the calculated results to the measured A-R-T spectra of the p-type GaAs samples. The total DF including the IVB contributions yields the refractive index and extinction coefficient by which the values of A and R were calculated using the ITMM. A good agreement between the theoretical and experimental spectra was achieved as shown in Fig. 2. Table III and Fig. 3 list the fitting parameters. As the so-lh transitions are relatively weak compared with other IVB transitions, the broadening constant cannot be well determined and was thus, assumed to the same as the so-hh transition. In view of the results, the so-hh transition has a larger broadening constant than the lh-hh transition. The difference is enlarged in highly doped samples where the line-shape of the lh-hh transition remains in contrast to the nearly invisible so-hh peak (Fig. 7). As a result of the shifting deep into the VBs of the Fermi level, Δ_c slowly increases with the increasing of doping concentrations (Fig. 3). This is reasonable since the energy of transitions occurring around the Fermi surface shifts toward the higher values. As can be seen in Fig. 3, the strength parameter A_{12} for the lh-hh transition increases at the high doping levels. Assuming doping in the materials without changing the VB structure (rigid band structure), for p-type GaAs at room temperature the Fermi level lies below the VB top when the doping level is greater than $8 \times 10^{18} cm^{-3}$. The resultant effect is a high amount of holes being populated into the high-energy states. At $p = 3 \times 10^{19} cm^{-3}$, the k values of the energy states around the Fermi surface correspond to the wave vectors at which the lh and hh bands start to run in parallel [see Fig. 1(b)]. The associated transitions thus, produce a higher value of strength since A_{12} [Eq. (6)] is proportional to the inverse difference in the hh and lh effective mass.

TABLE III. Fitting parameters for computing the contributions of IVB transitions to the DF. p denotes the doping concentration (in cm^{-3}). Also see Fig. 3 for doping dependent parameters.

	p-GaAs	p-$Ge_{0.98}Sn_{0.02}$
A_{12}($10^{-3}eV^2cm^3$)	Fig. 3	Fig. 3
Γ_{12}/σ_{12} (meV)	$39.2 + 0.15p/10^{18}$	$29.7 + 0.27p/10^{18}$
A_{13}($10^{-3}eV^2cm^3$)	2.2 ± 0.1	0.7 ± 0.1
Γ_{13}/σ_{13} (meV)	$36.0 + 1.63p/10^{18}$	$24.1 + 1.41p/10^{18}$
A_{23}($10^{-3}eV^2cm^3$)	10 ± 5	18 ± 5
Γ_{23}/σ_{23}(meV)	$36.0 + 1.63p/10^{18}$	$24.1 + 1.41p/10^{18}$
m_{hh}^*(m_e)	0.53^a	0.34^b
m_{lh}^*(m_e)	0.08^a	0.043^b
m_{so}^*(m_e)	0.15^a	0.095^b

[a]Reference 5.
[b]Reference 5, same as Ge (Ref. 5).
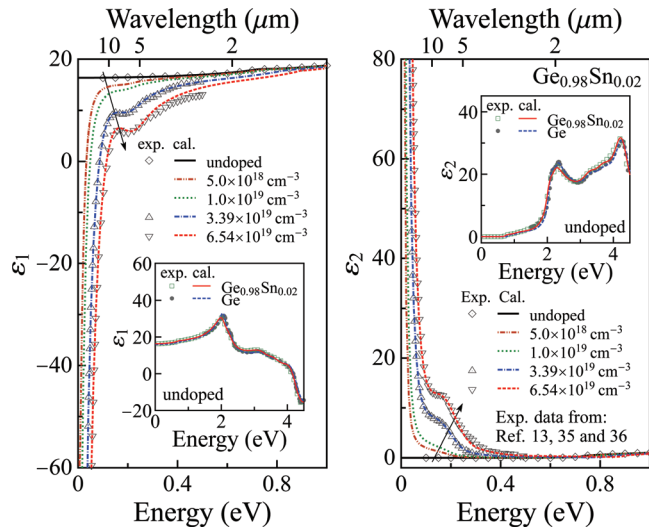
FIG. 5. (Color online) The comparison of experimental and calculated DF (ε_1 and ε_2) for p-type Ge$_{0.98}$Sn$_{0.02}$ at various doping concentrations, where the measured data are taken from Ref. 13. The insets show the calculated DF of undoped Ge and Ge$_{0.98}$Sn$_{0.02}$ in comparison with experimental data taken from Refs. 35 and 36. Notice that the contribution from the first phonon mode for the group IV semiconductors can be neglected.

Based on the fitting parameters, the total DF for a variety of doping concentrations up to 10^{20}cm^{-3} was calculated as shown in Fig. 4. The FC effects depress down the ε_1 in general. A strong feature at the low-energy side is due to the phonon absorption. According to the Drude term in Eq. (14), FC absorption exhibits a $1/E^2$ behavior which can be seen from the decreasing (or increasing) of the ε_1 (or ε_2) with reducing the photon energies. Both the FC and phonon absorption have the strong effects on the DF in the far infrared region, mostly greater than 10 μm. The IVB dominating range can be viewed approximately from the spin-orbit splitting energies, Δ_0 (0.224eV)[34] and Δ_1 (0.341eV)[23] for GaAs. The lh-hh transition primarily occurs below Δ_1, while the so-hh transition requires a higher photon energy than Δ_0. The so-lh transition is relatively weak due to the low occupation
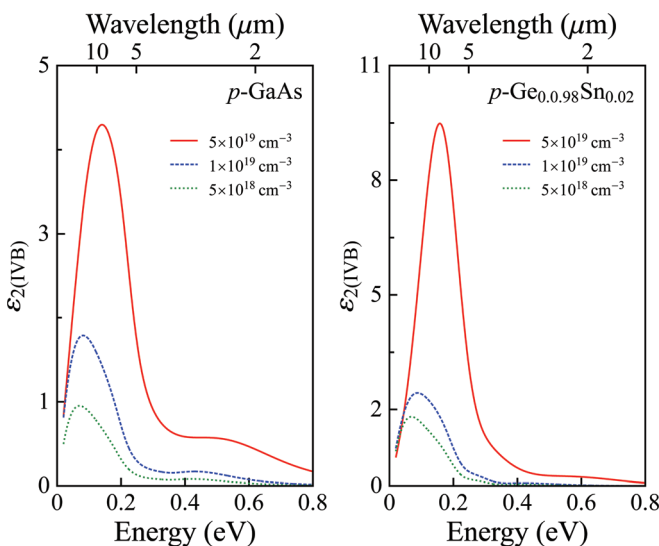
of the holes in the lh band. Therefore, the main region of IVB transitions is between 0.1–1.0 eV. The effects of IVB transitions on the variation of absorption and refractive index with the doping concentrations will be discussed in Sec. III C.

B. Application of the DF model to p-type Ge$_{1-y}$Sn$_y$

The investigation of optical properties on heavily doped p-type Ge$_{1-y}$Sn$_y$ was recently reported by D'Costa et al.[13] A direct measurement on the DF was performed using the infrared spectroscopic ellipsometry (SE). This material systems would be of interest in optical communication field as a reduction in bandgap of Ge can be achieved by increasing the Sn fraction. Additional advantages are the capability of growth on the Si substrate, which is favorable for realizing the monolithic OptoElectronic Integrated Circuit (OEIC). The investigation of the optical constants will favor such applications.

The DF model presented in Sec. II A is expected to be applicable to p-type Ge$_{1-y}$Sn$_y$ as its band structure (diamond type) resembles the one of GaAs (Zinc-blende type). The difference is the lack of inversion symmetry in the Zinc-blende semiconductors as compared with the diamond structures, which gives nonzero linear k terms in the E-k relationship when expanded into polynomial k terms around the VB top. This causes the maxima of the hh band slightly off the Γ point along the $\langle 111 \rangle$ direction. However, such a difference in band structure is indistinguishable in optical properties under investigation.

Using a similar procedure in the case of p-type GaAs, the DF parameters for BB transitions were firstly determined by fitting the experimental spectra of undoped materials taken from D'Costa's measurements.[35] Also a fit to undoped Ge using Aspnes's data[36] was carried out for comparison. Then IVB contributions were added to the model for p-type samples.[13] The resultant spectra are shown in Fig. 5. Table I, III and Fig. 3 summarize the fitting parameters. Notice that a fixed broadening constant for the E_0 transition was used here for p-type Ge$_{0.98}$Sn$_{0.02}$. The related effects cause the flattening of the E_0 transition and can be actually neglected when it comes to the region well below the fundamental bandgap. For comparison, the DF of two p-type Ge samples was also computed by fitting the absorption spectra taken from the works of Kaiser and Newman.[21,37] The difference in the DF and hence, the CP parameters between undoped Ge and Ge$_{0.98}$Sn$_{0.02}$ is small due to a small Sn fraction, as shown in insets of Fig. 5 and Table I. As can be seen in Fig. 3, the IVB broadening constants for p-type Ge samples follow the pattern of Ge$_{0.98}$Sn$_{0.02}$. However, the strength parameter A_{12} in p-type Ge$_{0.98}$Sn$_{0.02}$ increases with the doping as opposed to fixed values in p-type Ge. The reason is similar to the one previously discussed in the case of p-type GaAs (Sec. III A). An added effect is related to the presence of tensile strain ($\sim 0.15\%$) in the film. A strain can produce the warping[38] of hh and lh bands near the Γ point, which makes them almost parallel. When the doping level is high enough, a higher value of A_{12} can be resulted in terms of Eq. (6). This could be the reason for observing higher DF and the absorption coefficient of

FIG. 6. (Color online) The calculated DF (ε_2) with IVB contributions alone for p-type GaAs and Ge$_{0.98}$Sn$_{0.02}$ at different doping concentrations.

p-type $Ge_{0.98}Sn_{0.02}$ (shown in Figs. 6 and 7, respectively) in comparison with the same doping level of *p*-type GaAs.

The variation of the DF with the doping as shown in Fig. 5 is similar to the *p*-type GaAs, where the dominating IVB region is within 0.1–1 eV. The IVB effects will be further discussed in the following Section.

C. Effects of IVB transitions

The SE measurement has showed similar spin-orbit splitting energies of $Ge_{0.98}Sn_{0.02}$[35] to those of GaAs on the topmost VBs. Therefore, IVB transitions in both materials dominate the spectral range between 0.1–1.0eV as calculated by the DF model in Secs. III A and III B. The strength of IVB transitions is related to the concentration of the free holes and hence in competition with intra-band FC absorption.[12] The IVB contributions and FC absorption can be separated based on the present model. Figure 6 shows the calculated DF by IVB transitions alone. As GaAs and $Ge_{0.98}Sn_{0.02}$ have the similar spin-orbit splittings, the lh-hh and so-hh transitions cause individual peaks in the energy range for both materials, i.e., 0.1–0.3 eV and 0.4–0.8 eV, respectively. The total absorption coefficient is plotted in Fig. 7 where comparisons to experimental data show a good agreement. For samples with low doping levels, three peaks corresponding to the lh-hh, so-hh and so-lh transitions, respectively, can be identified. With increasing the doping, high damping occurs for the so-hh transition. The dependence of absorption coefficient on the doping concentrations exhibits a linear relationship shown in the insets of Fig. 7. As the absorption range spans a broad spectral region, the *p*-doped materials are of interest for infrared detection.[15,16]

For semiconductor device designs, an accurate model for the refractive index is crucial, e.g., for determining the optical field distribution in a structure. Stern[39] has considered the doping effects on the refractive index of *p*-type samples (for energies near the fundamental bandgap) by estimating IVB transiti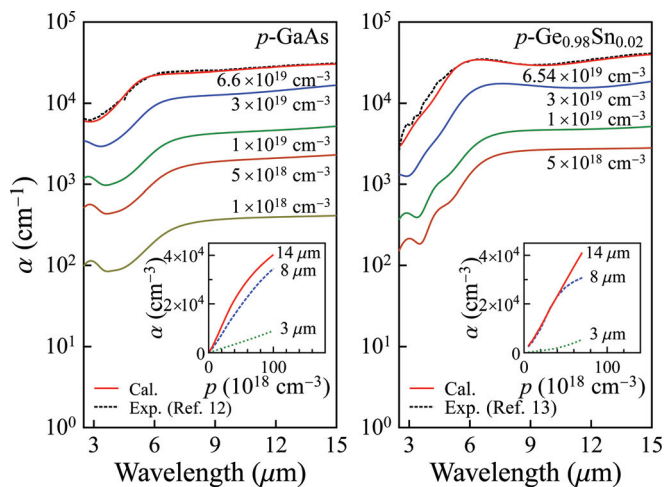ons from the limited experimental absorption data. Nevertheless, the estimation shows IVB contributions exceed the FC absorption. By using the DF model, the spectra of refractive index can be easily calculated as shown in Fig. 8. For the undoped GaAs, a good agreement between the theoretical and experimental values was achieved. With the doping, the refractive index is reduced with a strong reduction at high levels and low photon energies. Also shown is the data calculated by Huang *et al.*[40] for wavelengths at 1.06, 1.30 and 1.55 μm. A strong reduction when the photon energies shift toward low values is the result of high absorption either due to IVB transitions or due to FC absorption. For semiconductor devices, the operating wavelength could be selected at low absorption region where the index of refraction has a little change from the undoped materials. However, several crucial spectral regions, e.g., the 8–14 μm atmospheric window, fall into the IVB scope in which the refractive index are sensitive to the doping concentrations. Therefore, a proper consideration
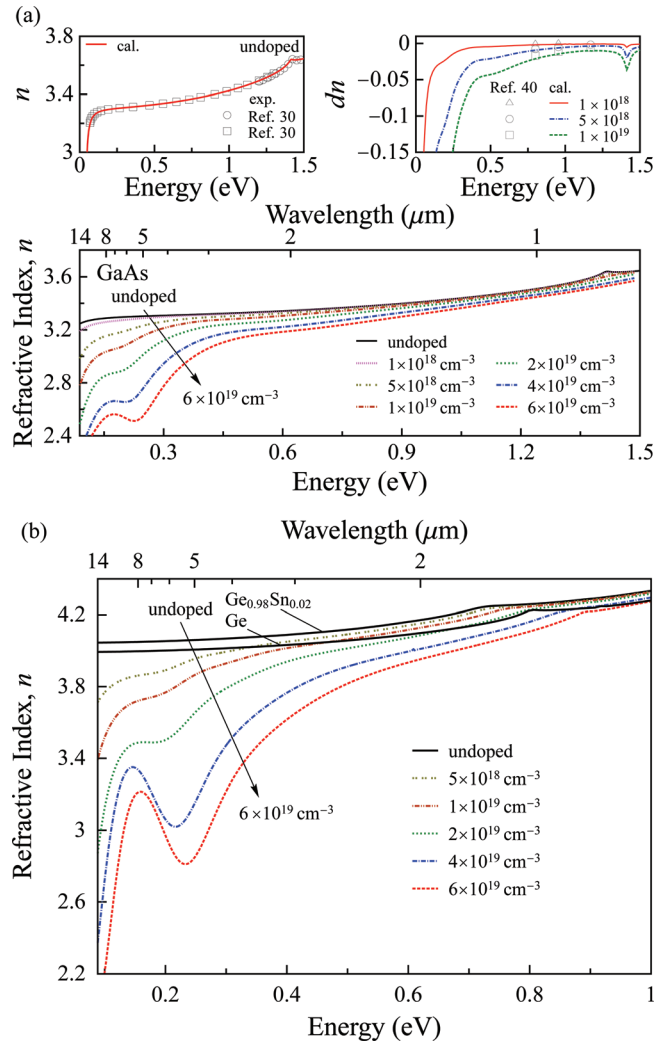
FIG. 8. (Color online) Calculated index of refraction for GaAs (a) and $Ge_{0.98}Sn_{0.02}$ (b). In the upper left figure of (a), a comparison was made to the data measured by Sell and Plotnichenko (Ref. 30). The difference in refractive index between the undoped and doped GaAs is shown in the upper right figure of panel (a). Also shown is the data from Ref. 40. A strong reduction in the refractive index in the low-energy region and higher doping samples is the result of increased absorption due to the FC and IVB processes.

FIG. 7. (Color online) Calculated absorption coefficient (α) for *p*-type GaAs and $Ge_{0.98}Sn_{0.02}$ at different doping concentrations. Also shown are the data from Refs. 12 and 13. The insets show the variation of absorption coefficient with the doping concentrations at 3, 8 and 14 μm.

with the IVB contributions is necessary. The presented DF model and yielded optical constants will be useful for modeling semiconductor structures.

IV. SUMMARY

To summarize, a DF model for IVB transitions has been deduced with the analytical expressions under the parabolic-band approximation. The model also incorporated contributions from BB transitions, FC and lattice absorption, each of which dominates at different spectral ranges. The total DF thus, determines related optical constants in the spectral range from the ultraviolet (UV) to the infrared (IR) region. The DF of p-type GaAs and $Ge_{1-y}Sn_y$ has been determined by fitting the experimental data, showing dominating IVB range between 0.1–1eV in accordance with the spin-orbit splitting energies of the VBs. The fitting to these two materials with different crystal structures shows the DF can be modeled under the parabolic-band approximation for doping levels up to $10^{20}cm^{-3}$. The model is also expected to be applicable to other group III-V and IV semiconductors since their valence band structures resemble the ones under investigation. The obtained DF and related optical constants, such as the absorption coefficient and the index of refraction, are useful for designing devices, such as p-type GaAs for infrared detection as recently demonstrated,[15,16] whereas, the applications of $Ge_{1-y}Sn_y$ for optoelectronic devices will need the optical constants as did in the work.

ACKNOWLEDGMENTS

[1] S. Adachi, Phys. Rev. B **35**, 7454 (1987).
[2] R. J. Elliott, Phys. Rev. **108**, 1384 (1957).
[3] C. Tanguy, Phys. Rev. Lett. **75**, 4090 (1995); C. Tanguy, Solid State Commun. **98**, 65 (1996).
[4] T. Holden, P. Ram, F. H. Pollak, J. L. Freeouf, B. X. Yang, and M. C. Tamargo, Phys. Rev. B **56**, 4037 (1997); M. Muñoz, K. Wei, F. H. Pollak, J. L. Freeouf, and G. W. Charache, ibid. **60**, 8105 (1999).
[5] P. Y. Yu and M. Cardona, Fundamentals of Semiconductors: Physics and Materials Properties (Springer-Verlag, Berlin, 2005).
[6] A. Perera, W. Shen, W. Mallard, K. Wang, and M. Tanner, Appl. Phys. Lett **71**, 515 (1997).
[7] A. L. Korotkov, A. G. U. Perera, W. Z. Shen, J. Herfort, K. H. Ploog, W. J. Schaff, and H. C. Liu, J. Appl. Phys. **89**, 3295 (2001).
[8] M. B. M. Rinzan, D. G. Esaev, A. G. U. Perera, S. G. Matsik, G. von Winckel, A. Stintz, and S. Krishna, Appl. Phys. Lett. **85**, 5236 (2004).
[9] Z. G. Hu, M. B. M. Rinzan, S. G. Matsik, A. G. U. Perera, G. von Winckel, A. Stintz, and S. Krishna, J. Appl. Phys. **97**, 093529 (2005); Z. G. Hu, M. Strassburg, N. Dietz, A. G. U. Perera, A. Asghar, and I. T. Ferguson, Phys. Rev. B **72**, 245326 (2005).
[10] R. Braunstein and L. Magid, Phys. Rev. **111**, 480 (1958).
[11] M. L. Huberman, A. Ksendzov, A. Larsson, R. Terhune, and J. Maserjian, Phys. Rev. B **44**, 1128 (1991).
[12] W. Songprakob, R. Zallen, W. K. Liu, and K. L. Bacher, Phys. Rev. B **62**, 4501 (2000); W. Songprakob, R. Zallen, D. V. Tsu, and W. K. Liu, J. Appl. Phys. **91**, 171 (2002).
[13] V. R. D'Costa, J. Tolle, J. Xie, J. Kouvetakis, and J. Menéndez, Phys. Rev. B **80**, 125209 (2009).
[14] A. G. U. Perera, H. X. Yuan, and M. H. Francombe, J. Appl. Phys. **77**, 915 (1995).
[15] P. V. V. Jayaweera, S. G. Matsik, A. G. U. Perera, H. C. Liu, M. Buchanan, and Z. R. Wasilewski, Appl. Phys. Lett. **93**, 21105 (2008).
[16] Y. F. Lao, P. K. D. D. P. Pitigala, A. G. U. Perera, H. C. Liu, M. Buchanan, Z. R. Wasilewski, K. K. Choi, and P. Wijewarnasuriya, Appl. Phys. Lett. **97**, 091104 (2010).
[17] A. Rogalski, Rep. Prog. Phys. **68**, 2267 (2005).
[18] E. O. Kane, J. Phys. Chem. Solids **1**, 82 (1956).
[19] J. B. Arthur, A. C. Baynham, W. Fawcett, and E. G. S. Paige, Phys. Rev. **152**, 740 (1966).
[20] A. H. Kahn, Phys. Rev. **97**, 1647 (1955).
[21] R. Newman and W. W. Tyler, Phys. Rev. **105**, 885 (1957).
[22] S. L. Chuang, Physics of Optoelectronic Devices (Wiley, New York, 1995).
[23] I. Vurgaftman, J. R. Meyer, and L. R. Ram-Mohan, J. Appl. Phys. **89**, 5815 (2001).
[24] T. B. Bahder, Phys. Rev. B **41**, 011992 (1990).
[25] S. Shokhovets, G. Gobsch, and O. Ambacher, Phys. Rev. B **74**, 155209 (2006).
[26] P. Rees and P. Blood, Semicond. Sci. Technol. **10**, 1545 (1995).
[27] M. Born and E. Wolf, Principles of Optics: Electromagnetic Theory of Propagation, Interference and Diffraction of Light, 7th ed. (Cambridge University Press, 1999).
[28] S. Zollner, J. Appl. Phys. **90**, 515 (2001).
[29] P. P. Paskov, J. Appl. Phys. **81**, 1890 (1997).
[30] D. D. Sell, H. C. Casey, and K. W. Wecht, J. Appl. Phys. **45**, 2650 (1974); V. G. Plotnichenko, V. O. Nazaryants, E. B. Kryukova, and E. M. Dianov, J. Phys. D: Appl. Phys. **43**, 105402 (2010).
[31] S. Adachi, Physical Properties of III-V Semiconductor Compounds: InP, InAs, GaAs, GaP, InGaAs, and InGaAsP (Wiley, New York, 1992).
[32] R. Braunstein and E. Kane, J. Phys. Chem. Solids **23**, 1423 (1962).
[33] M. Sotoodeh, A. H. Khalid, and A. A. Rezazadeh, J. Appl. Phys. **87**, 2890 (2000).
[34] P. Lautenschlager, M. Garriga, S. Logothetidis, and M. Cardona, Phys. Rev. B **35**, 9174 (1987).
[35] V. R. D'Costa, Y. Fang, J. Mathews, R. Roucka, J. Tolle, J. Menéndez, and J. Kouvetakis, Semicond. Sci. Technol. **24**, 115006 (2009); V. R. D'Costa, C. S. Cook, A. G. Birdwell, C. L. Littler, M. Canonico, S. Zollner, J. Kouvetakis, and J. Menéndez, Phys. Rev. B **73**, 125207 (2006).
[36] D. E. Aspnes and A. A. Studna, Phys. Rev. B **27**, 985 (1983).
[37] W. Kaiser, R. J. Collins, and H. Y. Fan, Phys. Rev. **91**, 1380 (1953).
[38] A. Afzali-Kushaa and G. I. Haddad, J. Appl. Phys. **77**, 6549 (1995).
[39] F. Stern, Phys. Rev. **133**, A1653 (1964).
[40] H. C. Huang and S. Yee, J. Appl. Phys. **70**, 925 (1991).
[41] A. Baldereschi and N. C. Lipari, Phys. Rev. B **3**, 439 (1971).
[42] M. Cardona, K. L. Shaklee, and F. H. Pollak, Phys. Rev. **154**, 696 (1967).